Methane Assisted Chemical Looping Water Splitting Performance of $Sr_2FeMo_{0.6}Ni_{0.4}O_{6-\delta}$ Double Perovskite for Solar Fuels Production

Andrea Strazzolini[1] [iD], Francesco Orsini[2*] [iD], Salvatore F. Cannone[2] [iD],
Domenico Ferrero[2] [iD], Marta Boaro[1] [iD], Jordi Llorca[3] [iD], Georgios Dimitrakopoulos[4,5] [iD],
Alessandro Trovarelli[1] [iD], Massimo Santarelli[2] [iD], and Ahmed F. Ghoniem[4] [iD]

[1] Polytechnic Department of Engineering and Architecture (DPIA), University of Udine, Via Cotonificio 108, Udine 33100, Italy.

[2] Energy Department (DENERG), Politecnico di Torino, Corso Duca degli Abruzzi 24, Torino 10129, Italy.

[3] Institute of Energy Technologies, Department of Chemical Engineering, and Barcelona Research Center in Multiscale Science and Engineering, Universitat Politècnica de Catalunya, EEBE, Eduard Maristany 10-14, 08019 Barcelona, Spain.

[4] Department of Mechanical Engineering, Massachusetts Institute of Technology, Cambridge, MA 02139, USA.

[5] Exponent, Inc., Natick, MA, 01760, USA.

*Correspondence: Francesco Orsini, francesco.orsini@polito.it

Abstract. In this work, we performed a preliminary investigation on the redox behaviour of $Sr_2FeMo_{0.6}Ni_{0.4}O_{6-\delta}$ (SFMN) double perovskite in H_2-H_2O and CH_4-H_2O redox cycles in order to explore the potential use of this oxide as an Oxygen Carrier (OC) in fuel-assisted Chemical Looping Water Splitting (CLWS) processes driven by concentrated solar energy. The results were compared with our previous findings on the Reverse Water Gas Shift Chemical Looping (RWGS-CL) reaction. The improvement in performance due to the bimetallic exsolution on the OC surface is observed. This OC exhibits interesting activity and stability over CH_4-assisted CLWS cycling. Future investigations are planned to examine the structural transformations that might impact the redox behaviour of this material in water splitting processes.

Keywords: Chemical Looping; Perovskite; Exsolution; Water Splitting; Solar Fuels; CH_4 Reforming.

1. Introduction

The urgency of climate change calls for the development of alternative energy pathways to replace fossil fuels with energy renewable sources. Among these, solar energy is the most abundant and could potentially meet the world's energy needs. The intermittent nature of solar energy and its conversion into fuels currently pose technological challenges. A promising route for the storage of solar energy relies on its conversion to chemicals, such as gaseous and liquid fuels, through thermochemical processes [1]. In this regard, Chemical Looping (CL) offers a versatile solution for the efficient conversion of solar thermal energy into fuels, *e.g.*, H_2 and syngas. CL uses a solid redox-active material to break up a thermochemical reaction into two steps, thus by separating reaction products, overcoming thermodynamic limitations, and minimizing exergy losses [2]. In CH_4-assisted Chemical Looping Water Splitting (CLWS), a solid Oxygen Carrier (OC) is employed to selectively oxidize CH_4 to H_2 and CO (reduction step, Equation (1)); subsequently, the OC lattice oxygen is restored by oxidation with H_2O (water splitting step, Equation (2)).

$$CH_4 + MeO_x \rightleftharpoons CO + 2H_2 + MeO_{x-1} \qquad (1)$$
$$H_2O + MeO_{x-1} \rightleftharpoons H_2 + MeO_x \qquad (2)$$
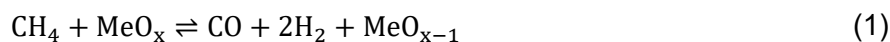
In this way, two separate streams, a syngas with a $H_2/CO \approx 2$, suitable for Gas-To-Liquid (GTL) processes [3], and a stream of pure H_2 are generated with a minimal energy penalty for separation. The overall methane steam reforming reaction is endothermic, and supplying the thermal energy required by the OC reduction step using a renewable source raises the energy content of the products by a factor of 1.28 over that of the reactants [1]. One of the most critical aspects in the process development is the selection of the OC material, since its chemical and mechanical performance over prolonged reduction-oxidation cycling determines the economics of the plant [4]. Perovskite-structured oxides (with general formula ABO_3) have shown desirable properties for CH_4-assisted CLWS, such as good thermal stability and a high syngas selectivity. Through doping the A-site and B-site, it is possible to effectively tune the concentration of surface lattice oxygen vacancies and the ionic conductivity, thus modulating the redox behavior of the OC [5]. Promising results in terms of stability and selectivity have been obtained by, *e.g.*, the development of core-shell metal oxide-perovskite composite OC materials [6] and by optimizing the composition to promote the exsolution of well-dispersed metallic nanoparticles that could act as catalyst [7], [8].

Sr-Fe-Mo-Ni perovskites (SFMN) with composition $Sr_2Fe_xMoNi_{1-x}O_{6-\delta}$ were recently investigated as catalyst for the Dry Methane Reforming (DMR) [9]. When exposed to high temperature (≈ 900 °C) in H_2 reducing atmosphere, this material exhibited a morphological activation inducing Ni_3Fe nanoparticles exsolution, able to catalyze the overall DMR. In exsolution, metal alloy nanoparticles grow from inside the structure instead of being deposited from the outside, ensuring better stability because the particles remain socketed into the support surface [10]. In a recent investigation by our group, $Sr_2FeMo_{0.6}Ni_{0.4}O_{6-\delta}$ double perovskite was investigated as OC in the CL Reverse Water-Gas Shift (RWGS-CL) reaction, in which the sample was reduced with H_2 and oxidized with CO_2 [11]. SFMN samples were tested *via* thermogravimetry (TGA) and in packed-bed reactor over a wide temperature range, 550 – 950 °C. The material was able to undergo isothermal RWGS-CL cycles, keeping a high CO production yield above 1.5 mmolCO/g after 326 redox cycles at 850 °C. This yield is comparable with or superior to most of the available performance throughout the literature. Exsolution of Ni-Fe alloy nanoparticles was observed and reported in several publications, and it determined the superior redox performance after the material activation.

In the present work, we investigate the role of the Ni_3Fe exsolution on CH_4-assisted CLWS redox cycles and compare the results with H_2-assisted CLWS and with previous experimental campaign on RWGS cycles.

2. Materials and Methods

SFMN powder was prepared and characterized by X-ray diffraction (XRD) and High-Resolution Transmission Electron Microscopy (HRTEM), at the structural and nanoscale, respectively, as described in our recent study [11].

H_2-assisted CLWS cycles were carried out with an Autochem II 2920 Micromeritics Analyzer equipped with a Thermal Conductivity Detector (TCD). One cycle consisted of a reduction step with a temperature-programmed heating ramp of 10 °C/min starting at the room temperature (RT) and up to 850°C, using 5% H_2 in N_2 flow at 35 Nml/min, as a reductant. The sample was idled for 1 h at the final conditions, then purged with N_2 before of the oxidation step. The latter was performed by pulses of water vapor (injected through a 500 µl loop filled from a saturator operating at 70 °C and 35 Nml/min He flow), to achieve a steady state for H_2 production. The sample was then completely oxidized with air at 500 °C for 30 min, and then cooled down to room temperature to repeat the cycle.

Temperature-Programmed Reduction (TPR) in CH_4 atmosphere was conducted in a thermogravimetric analyser (TGA) (STA 2500 Regulus, Netzsch, Germany), both on a pristine

SFMN sample and on a pre-treated sample. For the pretreatment, aimed at promoting metal exsolution, a 30 mg sample was loaded into a packed-bed reactor, and the sample was kept in 10% H_2/N_2 at 850 °C for 2 h with gas flow rate of 200 Nml/min. Then, the reactor was cooled down in 100% N_2 to ambient temperature, prior to CH_4-TPR in the TGA. The total gas flow rate in the TGA was kept constant at 80 Nml/min. The temperature was first raised from room temperature to 850 °C (20 °C/min) in 100% Ar, and the sample was oxidized at 850 °C in 50% air/Ar (synthetic air composition: 20% O_2, 80% N_2) for 30 min. Then, after it was cooled down back to 250 °C (20 °C/min) in 100% Ar, and maintained at 250 °C for 10 min, the TPR was initiated and performed from 250 °C up to 850 °C (10 °C/min), under a 2.5% CH_4/Ar mixture. CH_4 concentration was maintained low for safety reasons. Finally, the temperature was rapidly decreased back to room temperature in 100% Ar. Isothermal reduction at 850 °C was avoided to limit CH_4 cracking and carbon deposition.

CH_4-assisted CLWS cycles were run isothermally at 850 °C. A sample of 100 mg was loaded onto a microreactor connected to a calibrated mass spectrometer. Each cycle consisted in a 10 min reduction 5% CH_4/He and a 20 min oxidation with 6% H_2O/He, with a 5 min purge in between. The inlet flow rate in the microreactor was kept constant at 50 Nml/min, obtaining a GHSV ≈ 20.000 h^{-1}. The amount of solid carbon deposited on the sample upon exposure to CH_4 was determined from the evolved amounts of CO and CO_2 during the steam oxidation step. To exclude the formation of stable carbon deposits, at the end of each test the samples were kept in air at 850 °C for 30 minutes, and carbon oxidation products were monitored. For all tests, negligible amounts of CO and CO_2 were detected.

3. Results and Discussion

3.1 H_2-assisted Chemical Looping Water Splitting

Before studying the behaviour of SFMN in the CH_4-assisted CLWS, the water splitting performance and the material stability in water vapor were investigated through multiple H_2-TPR – H_2O isothermal oxidation cycles at 850 °C. H_2 is used as a reducing agent instead of CH_4 with the aim of exploring the material redox activity without handling carbonaceous species and thus by-passing cracking and deposition phenomena which can complicate the investigation and affect performance [12]. Figure 1, with H_2-TPR on the left (Figure 1a) and water splitting on the right (Figure 1b), shows the results of some representative cycles. The first TPR shows two partially overlapping signals with maxima at 460 and 485 °C, that were attributed to the reduction of surface Ni^{2+} and Fe^{4+} cations and to the reduction of high-valence cations into the bulk (Mo^{6+}, Fe^{3+} and Ni^{2+}), respectively [11], [12], [13]. The high-temperature signal starting around 700 °C can be ascribed to the reduction of Fe^{2+} to Fe^0 and to the progression of structural changes in the perovskite lattice. In the second reduction, a large H_2 consumption peak is observed centred at 420 °C, with a small shoulder around 500 °C. Compared to the first TPR, the H_2 consumption below 600 °C is increased by 52%. The higher H_2 consumption in the 300-480 °C range can be attributes to the increased reducibility of Ni^{2+} and Fe^{3+} cations and the increased content of the Ruddlesden-Popper (RP) phase $Sr_3FeMoO_{7-\delta}$ in the sample following the irreversible structural transformations that took place during the first reduction, as discussed by Felli et al. [13]. Given the higher reducibility at low to intermediate temperatures, a decrease in the high temperature contribution is observed. The following cycles show the same features as the second cycle, and the total hydrogen consumption stabilizes from the fourth cycle onwards (Table 1). Hydrogen production during the water splitting step also improved at the second cycle and stabilized at the fourth cycle. The corresponding H_2 yield of the cycles was of 50%. This is probably due to the instrumental constraints that do not allow to obtain high concentration of water vapour in each pulse, thus ending up with an equilibrium oxygen partial pressure that allows the stabilization of the nonstoichiometric phases of perovskites formed, rather than their complete oxidation. Further studies are needed to confirm this hypothesis. Thus, SFMN appears to be stable in the H_2-assisted CLWS cycles, reaching a steady state after four cycles. This behaviour is different from the results obtained in our previous study under RWGS-CL conditions [11], in which the CO_2-oxidized material reached a steady state in the CO yield after around forty cycles.
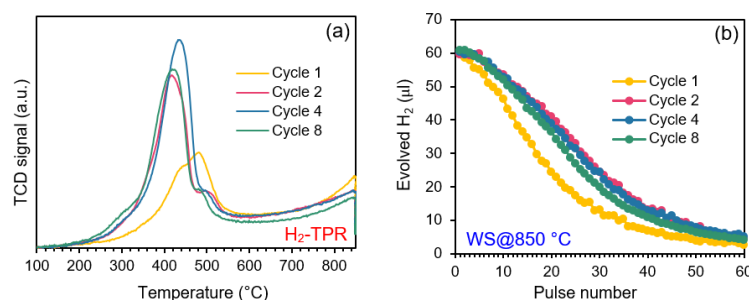
Figure 1. H_2-assisted CLWS cycles. (a) H_2-TPR up to 850 °C. (b) Water splitting at 850°C.

Table 1. Comparison of H_2 consumption, H_2 yield and H_2 production/consumption ratio referred to the selected H_2-TPR – WS cycles.

Cycle number	H_2 consumed (mL/g)	H_2 produced (mL/g)	% of oxidation
1	53.8	24.1	44.8
2	59.4	33.5	56.4
4	64.1	32.1	50.0
8	63.4	31.5	52.6

3.2 CH₄-assisted Chemical Looping Water Splitting

The SFMN reactivity towards partial oxidation of methane was preliminarily explored *via* CH_4-TPR in the TGA, comparing the reduction extent and the DTG-based reduction rate in the pristine and pretreated samples, with the latter being representative of an exsolved material [11]. The thermograms are depicted in Figure 2a. The 100% oxidized mass is taken as the stabilized post-oxidation value at 250 °C, just before starting the TPR ramp. While the mass signal is the same for the two samples up to around 700-730 °C, the pretreated sample clearly shows improved reactivity towards methane from 750 °C on, with a consistently higher mass loss (red solid curves) and notably higher DTG-based reduction rate (red dashed curves). This suggests that the exsolved material can achieve higher CH_4 conversion. XRD spectra of the two tested samples, shown in Figure 2b-c-d, highlight the presence of the Ni-Fe alloy and of the RP phase in the pretreated specimen, consistent with previous results, together with a wider shoulder at around 44° 2θ. An incipient Ni_3Fe peak at 44.5° 2θ can be also observed in the pristine sample, likely resulting from exposure to the CH_4 reducing atmosphere at increasing temperature. However, a concomitant RP phase was not detectable.
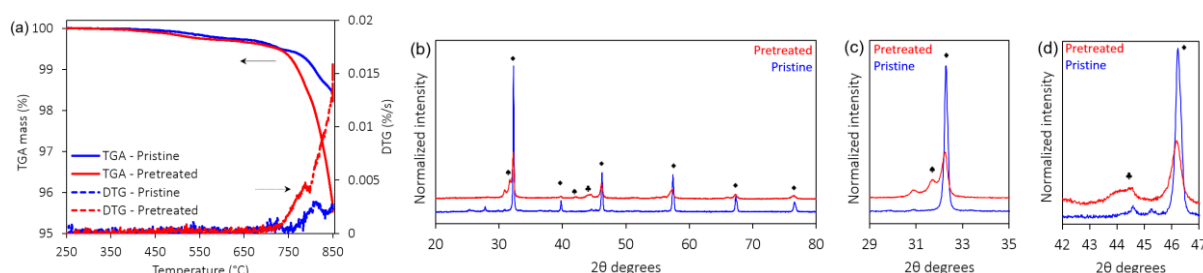

Figure 2. (a) CH_4-TPR in a TGA on pristine and pretreated samples. (b, c, d) XRD spectra of the two samples tested in TGA: (b) Full spectra. (c) Detail of the 30-35 2θ range. (d) Detail of the 42-47 2θ range. Ni_3Fe (♣), RP-phase Sr_3FeMoO_6 (♠), Sr_2FeMoO_6 (♦).

Given the high reactivity observed towards methane at 850 °C, SFMN reducibility in CH_4 was investigated in isothermal CH_4-H_2O cycles in a fixed bed microreactor at this temperature, which was also previously identified as suitable for long isothermal cycling in RWGS-CL conditions [11]. Firstly, the reducibility in a CH_4-containing atmosphere was compared to H_2-assisted reduction in Figure 3. This was done by performing five CLWS cycles using 5% H_2 as reducing agent and ten cycles using 5% CH_4. The test was preceded by a 2 h reduction with

5% H_2/He at the same temperature, to induce the exsolution of the Ni-Fe alloy nanoparticles, followed by a 30 min oxidation with 5% O_2/He. The constant response obtained in the five H_2-H_2O cycles confirmed that the transformation has reached a steady state, leading to the production of approximately 2.5 $mmolH_2$/g in each cycle (Figure 3a). During the CH_4-H_2O cycles the duration of the reduction step was limited to 10 min to limit carbon deposition, which could induce loss of activity and complicate further sample analysis. Despite this precaution, some carbon was deposited on the OC (Figure 3b), and its subsequent gasification by reaction with steam generated initially a higher amount of H_2 than that obtained in H_2-assisted cycles, also reducing its purity. It is worthy to note that the formation and subsequent gasification of carbon progressively diminished through the cycles, and the H_2 yield upon oxidation approached the same value obtained with H_2-H_2O cycles after 10 cycles. In the last cycle, 2.76 mol of H_2 were produced per mole of converted CH_4, of which 1.73 mol_{H2}/mol_{CH4} from the reduction step, and 1.03 mol_{H2}/mol_{CH4} from the water splitting step. CO selectivity was higher than 90% in all the reduction steps, as evidenced in Figure 3b.
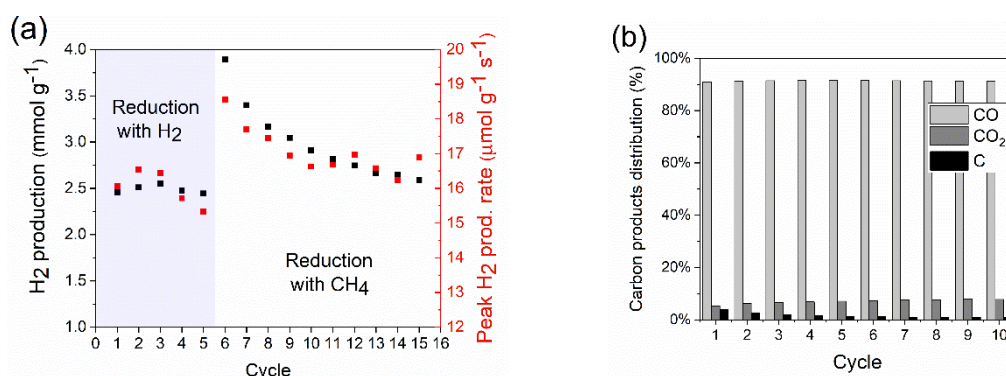

***Figure 3**. Comparison of SFMN performance between H_2-assited and CH_4-assisted reduction. (a) H_2 yield (black squares) and H_2 production rate (red squares) upon H_2O oxidation. (b) Carbon products distribution upon CH_4-assisted reduction.*

The effect of the microstructure evolution during the CH_4-assisted reduction at high temperature was investigated by exposing the as-synthesized sample directly to CH_4-H_2O cycles at 850 °C, without previous pretreatment. Results are shown in Figure 4. Both H_2 yield and its production rate increase steadily in the first seven cycles, after which they stabilize at the same value obtained with H_2 pretreated samples (2.5 $mmolH_2$/g and 17 $\mu molH_2$/g/s, respectively, Figure 4a). This shows that SFMN transforms upon cycling, similarly to what was observed in the CH_4-TPR, and that exposure to CH_4 can induce exsolution as well (peak at 44.5° 2θ well matching the Ni_3Fe alloy, blue spectrum in Figure 2d). This is also consistent with the observation that the pretreated sample ensures a higher reactivity towards methane (Figure 2a). In a similar fashion, CO selectivity during the reduction step grew from 75% to >90% in the first cycles (Figure 4b). The latter phenomenon was attributed to the gradual depletion of highly active surface oxygen species, which could not be restored by steam oxidation. The concentration of surface oxygen vacancies is the main factor affecting CO selectivity of iron-based OCs when reacting with carbonaceous fuels [14], [15], [16], [17]. The H_2 yield of 2.5 $mmolH_2$/g observed here is higher than the corresponding long-cycling CO production of 1.5 $mmolCO$/g estimated in our previous work on RWGS-CL, while the fuel production rate is comparable, with around 17 $\mu molH_2$/g/s against 15 $\mu molCO$/g/s maintained after 300+ RWGS-CL cycles. The steady state CH_4-H_2O cycles seems to be reached in the first ten cycles, similarly to what happens in the preliminary study with H_2-H_2O (see Figure 1).

To have a quantitative idea on how SFMN performs with respect to alternative OCs, we compared its performance with previous works from the literature, as summarized in Table 2. The H_2 yield observed here (2.5 $mmolH_2$/g) is higher than several OCs proposed previously. Some of the reported OCs show a higher H_2 yield during the oxidation step at similar temperatures (e.g., 3DOM $LaFe_{0.9}Ni_{0.1}O_3$ and $BaCoO_3$/CeO_2), but also a lower H_2 purity at the same time. $CuFeO_4$ reported an outstanding H_2 yield during oxidation, but the CO selectivity (total,

including solid carbon deposition) during reduction is relatively low (<60%), against a value higher than 93% for SFMN. Similar considerations apply for $La_{1.6}Sr_{0.4}FeCoO_6$, that reaches a higher H_2 yield, but a much lower total CO selectivity (40%). Thus, overall, SFMN can be considered a promising candidate for CH_4-assisted CLWS.
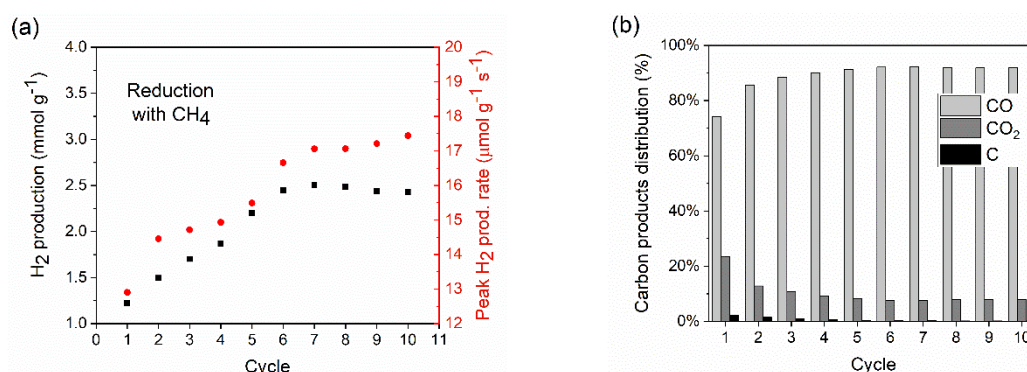

Figure 4. *Effect of progressive exposure to CH_4 on SFMN performance, without previous pre-treatment in H_2. (a) H_2 yield (black squares) and H_2 production rate (red squares) upon H_2O oxidation. (b) Carbon products distribution upon CH_4-assisted reduction.*

Table 2. *Comparison between SFMN and OCs from the literature in CH_4 assisted chemical looping water splitting. The works were collected from comprehensive reviews [18], [19].*

	Oxygen carrier	T (°C)	H_2 from H_2O (mmol/g)	H_2 purity (%)	Syngas prod. (mmol/g)	CO selectivity (%)	Cycles
Ce-based oxides	$5\%_{wt}$Ni CeO_2-TiO_2/$Ce_2Ti_2O_7$	900	2.1	~100	n.a.	85*	10
	$Ce_{0.5}Fe_{0.5}O_{2-\delta}$	850	3.72	~100	7.94	>85**	10
	Mg-Al supported Ce-Fe-Zr-O	850	0.92	~100	1.87	>80 (*/** n.a.)	20
	CeO_2/3DOM $LaFeO_3$	800	3.38	>99	9.94	90*	30
	$Ce_{0.8}Zr_{0.2}O_2$	800	1.88	n.a.	n.a.	76.73*	10
Perov-skites	$LaCo_{0.6}Fe_{0.4}O_3$	700	2.22	99.3	3.36	92**	20
	$La0.5Ce0.5FeO_3$	925	0.6	>95	0.75	>70*	100
	$La_{0.85}MnFe_{0.15}O_3$	850	0.55	~100	3.78 (1st cycle)	~99* (1st cycle)	20
	$LaMnO_{3+\delta}$	850	0.22	~100	0.51	89**	20
	$LaMn_{0.7}Fe_{0.3}O_{3+\delta}$	850	0.53	~100	1.67	96**	20
	$LaMn_{0.8}Co_{0.2}O_{3+\delta}$	850	0.81	~100	2	93.9**	20
	3DOM $LaFe_{0.2}Co_{0.8}O_3$	850	4.84	n.a.	n.a.	~100**	1
	$La_{1.6}Sr_{0.4}FeCoO_6$	850	5.9	n.a.	10.25	40*	20
	3DOM $LaFe_{0.9}Ni_{0.1}O_3$	850	6.39	84.3	n.a.	n.a.	10
	$BaCoO_3$/CeO_2	860	3.9	94.3	11.84	94.3**	25
Ferrites	$CuFe_2O_4$	900	11.3	>99	9.3	58.9*	5
This work	$Sr_2FeMo_{0.6}Ni_{0.4}O_{6-\delta}$	850	2.5	>99	6.73	>93*	10

*Total selectivity (including solid carbon).
**Gas-phase selectivity (excluding solid carbon).

Figure 5 reports the XRD spectra of SFMN samples as pristine, after ten H_2-H_2O and after ten CH_4-H_2O cycles. In both CL schemes, the prolonged cyclic exposure of SFMN to a reducing atmosphere at 850 °C induces the appearance of the Ni_3Fe peak at 44.5° 2θ and of the RP phase $Sr_3FeMoO_{7-\delta}$ at 31.5° 2θ [20], although the RP phase $Sr_3FeMoO_{7-\delta}$ at 31.5° 2θ is not clearly visible in the CH_4-H_2O cycled sample and manifests with a broadening of the peak rather than with an evident shoulder. The presence of $SrCO_3$ and $SrMoO_4$ can be due either to the interaction of residual carbonaceous deposits with the perovskite, or to the prolonged exposure to air of the sample before the XRD analysis, as previously observed [11]. Overall, these observations are consistent with the literature in which the exsolution was demonstrated

to take place in different reducing conditions in terms of pO_2 and the reducing gas and proved the effectiveness of the CH_4 atmosphere in promoting exsolution of Ni [21], [22].
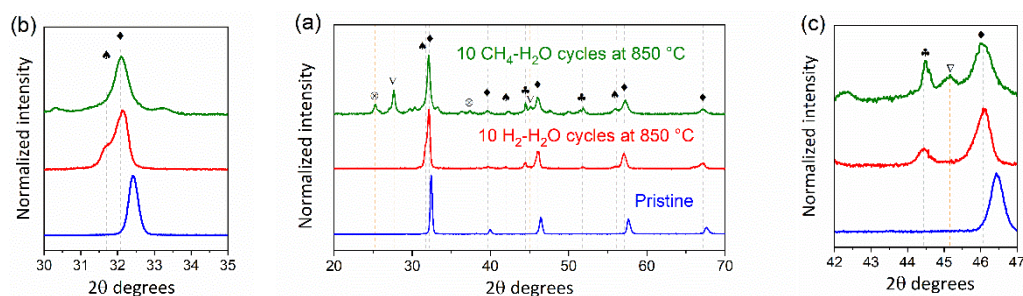

Figure 5. XRD profiles of SFMN as synthesized (blue), after ten H_2/H_2O cycles at 850 °C (red) and after ten CH_4/H_2O cycles at 850 °C (green). Ni_3Fe (♣), RP-phase Sr_3FeMoO_{7-d} (♠), Sr_2FeMoO_6 (♦), $SrCO_3$ (⊗), $SrMoO_4$ (▽). (b) Detail of the 30-35° 2θ range. (c) Detail of the 42-47° 2θ range.

4. Conclusions and Perspectives

In this study we demonstrate that SFMN is a valuable OC for CLWS processes and that exsolution can be promoted by CH_4 as well as by H_2, without experiencing much detrimental effect from carbon formation. The results were compared with those observed in RWGS-CL process previously published, showing some differences in terms of stability. The yield of CH_4-H_2O cycles seems to stabilize faster after ten cycles. Future work will include closer examination of the CH_4-assisted reduction cycles, along with the exsolution under water splitting conditions and its role on the redox performance, both in terms of reactivity and stability.

Data availability statement

Data will be made available on request.

Author contributions

AS: Conceptualization, Data Curation, Investigation, Methodology, Writing – Original Draft. FO: Data Curation, Investigation, Writing – Original Draft. SC: Conceptualization, Investigation, Resources, Writing – Review & Editing. MB: Conceptualization, Investigation, Resources, Writing – Review & Editing. DF, JL, GD, AT, MS, AG: Writing – Review & Editing.

Competing interests

The authors declare that they have no competing interests.

References

1. P. T. Krenzke, J. R. Fosheim, J. H. Davidson, «Solar fuels via chemical-looping reforming», Solar Energy, vol. 156, pp. 48–72, Nov. 2017, doi: 10.1016/j.solener.2017.05.095.
2. L.-S. Fan, L. Zeng, W. Wang, S. Luo, «Chemical looping processes for CO2 capture and carbonaceous fuel conversion – prospect and opportunity», Energy Environ. Sci., vol. 5, fasc. 6, pp. 7254–7280, May 2012, doi: 10.1039/C2EE03198A.
3. D. J. Wilhelm, D. R. Simbeck, A. D. Karp, R. L. Dickenson, «Syngas production for gas-to-liquids applications: technologies, issues and outlook», Fuel Processing Technology, vol. 71, fasc. 1, pp. 139–148, Jun. 2001, doi: 10.1016/S0378-3820(01)00140-0.
4. P. Cho, T. Mattisson, A. Lyngfelt, «Defluidization Conditions for a Fluidized Bed of Iron Oxide-, Nickel Oxide-, and Manganese Oxide-Containing Oxygen Carriers for Chemical-Looping Combustion», Ind. Eng. Chem. Res., vol. 45, fasc. 3, pp. 968–977, Feb. 2006, doi: 10.1021/ie050484d.

5.   G. Voitic, V. Hacker, «Recent advancements in chemical looping water splitting for the production of hydrogen», RSC Adv., vol. 6, fasc. 100, pp. 98267–98296, Oct. 2016, doi: 10.1039/C6RA21180A.

6.   L. Neal, A. Shafiefarhood, F. Li, «Effect of core and shell compositions on MeOx@LaySr1−yFeO3 core–shell redox catalysts for chemical looping reforming of me-thane», Applied Energy, vol. 157, pp. 391–398, Nov. 2015, doi: 10.1016/j.apenergy.2015.06.028.

7.   S.-K. Otto, K. Kousi, D. Neagu, L. Bekris, J. Janek, I. S. Metcalfe, «Exsolved Nickel Nanoparticles Acting as Oxygen Storage Reservoirs and Active Sites for Redox CH4 Conversion», ACS Appl. Energy Mater., vol. 2, fasc. 10, pp. 7288–7298, Oct. 2019, doi: 10.1021/acsaem.9b01267.

8.   H. Poelman, V. V. Galvita, «Intensification of Chemical Looping Processes by Catalyst Assistance and Combination», Catalysts, vol. 11, fasc. 2, Art. fasc. 2, Feb. 2021, doi: 10.3390/catal11020266.

9.   A. J. Carrillo, J. M. Serra, «Exploring the Stability of Fe–Ni Alloy Nanoparticles Exsolved from Double-Layered Perovskites for Dry Reforming of Methane», Catalysts, vol. 11, fasc. 6, p. 741, Jun. 2021, doi: 10.3390/catal11060741.

10.   D. Neagu et al., «Nano-socketed nickel particles with enhanced coking resistance grown in situ by redox exsolution», Nat Commun, vol. 6, fasc. 1, Art. fasc. 1, Sep. 2015, doi: 10.1038/ncomms9120.

11.   F. Orsini et al., «Exsolution-enhanced reverse water-gas shift chemical looping activity of Sr2FeMo0.6Ni0.4O6-δ double perovskite», Chemical Engineering Journal, p. 146083, Sep. 2023, doi: 10.1016/j.cej.2023.146083.

12.   Z. Zhao, M. Uddi, N. Tsvetkov, B. Yildiz, A. F. Ghoniem, «Redox Kinetics Study of Fuel Reduced Ceria for Chemical-Looping Water Splitting», J. Phys. Chem. C, vol. 120, fasc. 30, pp. 16271–16289, Aug. 2016, doi: 10.1021/acs.jpcc.6b01847.

13.   A. Felli et al., «Sr 2 FeNi 0.4 Mo 0.6 O 6−δ Evolution for SOFC and SOEC Applications», J. Electrochem. Soc., vol. 170, fasc. 11, p. 114511, Nov. 2023, doi: 10.1149/1945-7111/ad06e7.

14.   J. Yang et al., «On the ensemble requirement of fully selective chemical looping methane partial oxidation over La-Fe-based perovskites», Applied Catalysis B: Environmental, vol. 301, p. 120788, Feb. 2022, doi: 10.1016/j.apcatb.2021.120788.

15.   O. Mihai, D. Chen, A. Holmen, «Chemical looping methane partial oxidation: The effect of the crystal size and O content of LaFeO3», Journal of Catalysis, vol. 293, pp. 175–185, Sep. 2012, doi: 10.1016/j.jcat.2012.06.022.

16.   Q. Shen et al., «Effect of Regeneration Period on the Selectivity of Synthesis Gas of Ba-Hexaaluminates in Chemical Looping Partial Oxidation of Methane», ACS Catal., vol. 9, fasc. 1, pp. 722–731, Jan. 2019, doi: 10.1021/acscatal.8b03855.

17.   Y. Liu et al., «Near 100% CO selectivity in nanoscaled iron-based oxygen carriers for chemical looping methane partial oxidation», Nat. Commun., vol. 10, fasc. 1, Art. fasc. 1, Dec. 2019, doi: 10.1038/s41467-019-13560-0.

18.   S. Das, A. Biswas, C. S. Tiwary, M. Paliwal, «Hydrogen production using chemical looping technology: A review with emphasis on H2 yield of various oxygen carriers», International Journal of Hydrogen Energy, vol. 47, fasc. 66, pp. 28322–28352, Aug. 2022, doi: 10.1016/j.ijhydene.2022.06.170.

19.   W. Chang et al., «Recent Advances of Oxygen Carriers for Hydrogen Production via Chemical Looping Water-Splitting», Catalysts, vol. 13, fasc. 2, p. 279, Jan. 2023, doi: 10.3390/catal13020279.

20.   Z. Du et al., «High-Performance Anode Material Sr2FeMo0.65Ni0.35O6−δ with In Situ Exsolved Nanoparticle Catalyst», ACS Nano, vol. 10, fasc. 9, pp. 8660–8669, Sep. 2016, doi: 10.1021/acsnano.6b03979.

21.   Z. Sun et al., «Recent advances in exsolved perovskite oxide construction: exsolution theory, modulation, challenges, and prospects», J. Mater. Chem. A, vol. 11, fasc. 34, pp. 17961–17976, Aug. 2023, doi: 10.1039/D3TA03292B.

22. D. Neagu et al., «In Situ Observation of Nanoparticle Exsolution from Perovskite Oxides: From Atomic Scale Mechanistic Insight to Nanostructure Tailoring», ACS Nano, vol. 13, fasc. 11, pp. 12996–13005, Nov. 2019, doi: 10.1021/acsnano.9b05652.